ACS Combinatorial Science

Technology Note

pubs.acs.org/acscombsci

High-Throughput Preparation of Hexagonally Ordered Mesoporous Silica and Gadolinosilicate Nanoparticles for use as MRI Contrast Agents

Nicholas M. K. Tse,[†,‡] Danielle F. Kennedy,[*,†] Bradford A. Moffat,[§] Nigel Kirby,[∥] Rachel A. Caruso,[†,‡] and Calum J. Drummond[†]

[†]CSIRO Materials Science and Engineering, Bag 10, Clayton, Victoria 3169, Australia

[‡]PFPC, School of Chemistry, The University of Melbourne, Melbourne, Victoria 3010, Australia

[§]The University of Melbourne, Department of Radiology, Parkville, 3050, Australia

[∥]Australian Synchrotron, 800 Blackburn Rd, Clayton, Victoria 3168, Australia

Supporting Information

ABSTRACT: The development of biomedical nanoparticulate materials for use in diagnostics is a delicate balance between performance, particle size, shape, and stability. To identify materials that satisfy all of the criteria it is useful to employ automated high-throughput (HT) techniques for the study of these materials. The structure and performance of surfactant templated mesoporous silica is very sensitive to a wide number of variables. Variables, such as the concentration of the structure-directing agent, the cosolvent and dopant ions and also the temperature and concentration of quenching all have an influence on the structure, surface chemistry, and therefore, the performance of the mesoporous silica nanoparticles generated. Using an automated robotic synthetic platform, a technique has been developed for the high-throughput preparation of mesoporous silica and gadolinium-doped silicate (gadoliniosilicate) nanoparticulate MRI contrast agents. Twelve identical repeats of both the mesoporous silica and gadolinosilicate were synthesized to investigate the reproducibility of the HT technique. Very good reproducibility in the production of the mesoporous silica and the gadolinosilcate materials was obtained using the developed method. The performance of the gadolinosilicate materials was comparable as a T_1 agent to the commercial MRI contrast agents. This HT methodology is highly reproducible and an effective tool that can be translated to the discovery of any sol–gel derived nanomaterial.

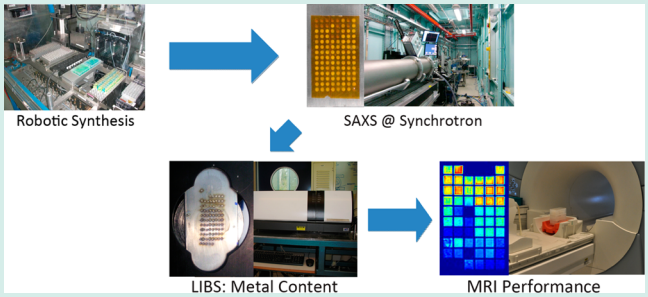

KEYWORDS: *high-throughput, mesoporous silica, nanoparticles, gadolinium, dynamic light scattering (DLS), small-angle X-ray scattering (SAXS), laser induced breakdown spectroscopy (LIBS), magnetic resonance imaging (MRI), Chemspeed*

The desire for rapid materials discovery has increased in recent years, in part driven by a need for application specificity.[1] Efficient design of high performance advanced materials requires a thorough understanding of the composition–property and structure–property relationships of the materials class at hand. In many cases, this knowledge can only be gained through the exploration of large arrays or libraries of samples, through a combination of careful experimental design and multivariate optimization. This is the main driver for the implementation of high-throughput (HT) approaches to materials discovery. Such discovery techniques have been employed for several decades by the biological research community and by the pharmaceutical industry focusing on the design and screening of small molecules.[2] Translation of these HT techniques to the discovery and development of materials has been slower to evolve.[3−6] To date, HT materials discovery has had a heavy emphasis on techniques that involved the production and characterization of material gradients.[7] Continuous compositional gradients cannot be readily generated for all materials. Another drawback to these investigations of compositional space across a gradient is that it can be difficult to reproduce the exact material specification from the region with the optimal performance once it is identified.[8]

In recent years, advancement in robotic synthesis platforms capable of handling solids, aggressive organic solvents, and corrosive reagents have enabled the translation of a number of different HT techniques into the field of materials discovery.[5,9] This increased chemical handling capability coupled with the ability to control the temperature, both well above and below physiological temperatures, means that there is now a large

Received: March 16, 2012
Revised: April 24, 2012
Published: June 7, 2012

ACS Publications © 2012 American Chemical Society

scope for the development of methods for the automated preparation of discrete libraries of materials, efficiently and effectively. The ability to generate "point-by-point" gradients where material properties can be measured from the matrix of discrete samples readily allows the mapping of desired properties against compositional space.[9]

Sol–gel-derived mesoporous materials are a class of materials that would benefit from the application of efficient HT techniques. In the discovery of sol–gel materials, there are numerous parameters that require optimization, but they can be broadly classified into chemical and environmental condition parameters. The chemical parameters include surfactant concentration, cosolvent, silica precursors, solvents, catalyst, pH range, and amount of dopant, and the variable parameters for the environmental condition are prehydrolysis time, synthesis temperature, quenching rate, and post-treatments. HT techniques combined with an appropriate design of experiment, allow the effective investigation of chemical space. Recently, Kreiter et al. reported the utilization of robotics in the preparation of sol solutions for the production of microporous silica membranes. They explored the effect of variables, such as temperature and silica precursor, on the structure of the cast membranes.[9]

In our targeted study, we use HT techniques for the development of mesoporous silicate nanoparticles for application as MRI contrast agents (CA). MRI CA can be classed as either T_1 or T_2 agents, with the former mainly gadolinium-based materials and the latter super paramagnetic iron oxide (SPIO) nanoparticles.[10,11] T_1 and T_2 agents have a brightening effect when used during a T_1 and T_2 scan, respectively. The synthesized materials in this work will be compared with the commercial agents, Omniscan and Magnevist. These agents are gadolinium chelated small molecules that have a typical r_1 and r_2 value of ~3 mM^{-1} s^{-1}.

We envision that the synthesis of mesoporous silicate nanoparticles with gadolinium doping may reduce the rate of tumbling of the paramagnetic species, increase gadolinium encapsulation and increase water exchange through the mesoporous network.[11] All of which are parameters associated with improved CA performance. Synthetic challenges arise from the fine balance between the careful sequestration of the cytotoxic gadolinium cations within the matrix of the nanoparticles and the maintenance of vacant coordination sites to facilitate the interaction of water with the paramagnetic gadolinium ions.[12] A balance between the concentration of the gadolinium, the surface area of the particle, the size and shape of the particles as well as the size and the shape of the water channels is needed. The factors involved in governing the above-mentioned properties are directly related to the amount of reagents and experimental parameters.[11,13]

The synthesis route used in this study for the preparation of the mesoporous silica materials is via an acid–base sol–gel method. The silica precursor is first prehydrolyzed followed by the addition of template agents and dopant. The mixture would then be quenched in an alkaline solution for the formation of nanoparticulate materials. In such case, the chemical parameters include surfactant concentration, co–solvent, silica precursors, solvents, catalyst (pH range), amount of dopant and experimental parameters are prehydrolysis time, synthesis temperature, quenching rate and post treatments.

In this study, we demonstrate the use of a Chemspeed Accelerator SLTII robotic synthesis platform for the synthesis of mesoporous silica-based nanoparticles. Twelve replicates of ordered mesoporous silicate were synthesized using the acid–base synthetic method.[13] The templating agent used in generating the mesopores in these nanoparticulate silicates was cetyltrimethylammonium bromide (CTAB). Furthermore, an additional twelve replicates were synthesized with gadolinium incorporated, to investigate the use of these materials as magnetic resonance imaging (MRI) contrast agents. The materials were characterized for variation in the ordering of the templated pores, and the particle size and polydispersity using small-angle X-ray scattering (SAXS) and dynamic light scattering (DLS), respectively. The metal content was characterized using laser induced breakdown spectroscopy (LIBS) and a commercial 3T MRI scanner was used for the relaxivity measurement.

RESULTS AND DISCUSSION

Developing a complete and integrated HT workflow for the discovery of application specific materials is key to the realization of the full benefit offered by HT techniques. Any workflow, however, is only as efficient and useful as the slowest step in the workflow. Recently, we have developed a whole suite of techniques for the discovery of mesoporous materials for medical imaging: design of experiments in multivariate space, characterization of their structural ordering (using HT SAXS/WAXS), screening for in vitro efficacy as MRI CAs[14] and plate based assays for the determination of particle size and the investigation of the fluorescent properties of the materials. The rate limiting step in the HT workflow for the development of these materials for application has long been the preparation of the functional sol–gel nanoparticles.

To address this, a HT approach to the preparation of silica-based nanoparticles has been developed using a Chemspeed Accelerator SLTII automated synthesis platform, Figure 1.

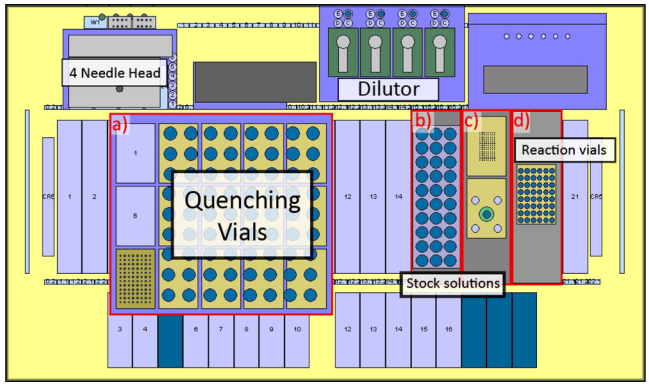

Figure 1. Screen capture of the experimental setup on the Chemspeed Accelerator SLTII robotic synthesis platform and the location of the sample wells in the block. The platform is laid out with a variety of sample holders: (a) a 15-position microtiter plate (MTP) orbital shaker; (b) one reagent rack housing 60 mL septa capped reagent vials; (c) one MTP/bottle holder; and (d) a temperature controlled magnetic stirrer fitted with a 48 position aluminum block for the temperature control of HPLC vials.

Using the automated synthesis procedure developed, a total of 12 replicate samples were prepared and characterized to determine the reproducibility of these templated materials at a miniaturized reaction scale using the robotic Chemspeed platform.

Hexagonally ordered mesoporous molecular sieves, MCM-41, were first demonstrated two decades ago, using CTAB as

dx.doi.org/10.1021/co300035q | ACS Comb. Sci. 2012, 14, 443–450

Table 1. Summary of Methods Reported to Synthesize Hexagonally Ordered Mesoporous Silicates, Doped Silicates, and Their Associated Physical Properties[a]

authors	template	acid−base	lattice type	unit cell size (nm)	pore size (nm)	particle size (nm)	dopant	ref
Beck et al.	CTAB	base	*P6mm*	4.0	3.7	50−200	n/a	15
Kapoor et al.	CTAB	acid−base	*P6mm*	4.4	2.5	<70	n/a	21
Fowler et al.	CTAB	base−acid	*P6mm*	4.9	n/a	60	n/a	22
Jiang et al.	CTAB	base	*P6mm*	4.4−4.6	n/a	1000	Al, Ce, Co, V, Zr	23
De Dood et al.	n/a	acid−base	core−shell	n/a	n/a	183−194	Eu, Tb	24
Lin et al.	CTAB	acid−base	*P6mm*	3.8	2.0	100	Gd, Eu, Tb	13
this work	CTAB	acid−base	*P6mm*	4.6	3.2	173	Gd	n/a

[a]n/a: not applicable; either no dopant was reported in work or no previously reported work.

the surfactant template under alkaline conditions.[15] Since then there has been a rapid expansion in the number of methods for the preparation of these types of ordered mesoporous silicates,[16,17] among which a variety of additives and dopants have been incorporated.[13,18,19] CTAB has remained a surfactant of choice as the hexagonal liquid crystalline phase it forms in aqueous solutions is robust in the presence of a variety of additives.[20] Therefore, in this work, this surfactant template was also chosen to demonstrate the autonomous synthesis of templated sol−gel materials.

The conventional MCM-41 methodology was modified in this work because under alkaline conditions the dopant of choice, gadolinium, readily forms insoluble gadolinium hydroxide. Sol−gel reactions of monomeric silica are versatile and can be conducted under both acidic and basic conditions; in fact the hydrolysis of silicic acid is accelerated under acidic conditions. Therefore, hydrolysis was first performed between all the reactants under acidic conditions. Association of the template, CTAB, with the fully hydrolyzed silicic acid ensured that upon quenching the reactants in an alkaline environment, the rate of condensation between the inorganic species would not be restricted by any unhydrolyzed ethyl groups. In addition, condensation of siliceous material under alkaline conditions promotes the formation of nanoparticulate morphology, unlike quenching in acidic conditions which facilities the formation of monoliths. Table 1 summarizes literature reports of metal incorporated silicates using a range of preparative methods. The acid−base sol−gel approaches combine the ability to incorporate a range of metal dopants into the matrix (an ordered-templated mesoporous silicate) with nanoparticulate morphology.

The silica sol−gel nanomaterials were prepared using a prehydrolysis/quenching method outlined by Lin et al. at a reduced scale.[13] The reagents were thoroughly mixed *via* stirring and allowed to stand for 25 min in acidic medium (pH 2) for TEOS (silica precursor) to be fully hydrolyzed. The prehydrolysis step is beneficial as this ensures the TEOS undergoes a more uniform condensation process during the subsequent quenching step in alkaline media.[25] The rate of the hydrolysis and condensation phases of sol−gel reactions can be separately controlled. Hydrolysis is optimal at pH $\leq$ 2; the isoelectric point of silicic acid.[26] Between pH 2−7, the hydrolysis and condensation processes are competitive. At pH $\geq$ 9, the condensation reaction takes preference over hydrolysis. The prehydrolysis step was employed to ensure that the silicic species had enough time to be thoroughly hydrolyzed and that the templating surfactant, CTAB, had sufficient time to undergo ion cooperative charge association with the inorganic ions: Si^{4-} and Gd^{3+}. Once complete hydrolysis was established, the rapid addition of the dilute ammonia solution to the prehydrolyzed solution quenches the reaction. The sudden change from acidic to basic conditions results in the formation of a nanoparticulate sol. Under alkaline conditions the silicate species tend to condense via a monomer-cluster mechanism leading to the formation of sol structures with a globular morphology; this is in contrast to the cluster−cluster mechanism, under an acidic environment, which generates sol particles with a more open fractal structure that resembles those found in gels. In addition, in alkaline conditions the dissolution-reprecipitation of the silicate species enables the sol product, after quenching, to structurally evolve into a more interconnected silicate matrix. Whereas under acidic conditions, the condensation is generally irreversible leaving the open fractal structure as is without the structural evolution to result in a globular sol structure.[26] Therefore, the quenching process enables the formation of nanoparticles. The presence of CTAB and the dopant, gadolinium, homogeneously mixed in the sol-mixture, gives rise to the final mesoporous gadolinosilicate nanoparticles. The nanoparticles were calcined at 500 °C for 10 h in air to remove the template molecules.

The pore ordering templated using the surfactant template, CTAB, was determined from the SAXS patterns. The materials were highly ordered with *P6mm* hexagonally arranged symmetry. Up to five reflections were observed for these materials, indicating that the pores have strong and persistent ordering and that there is a strong retention of the templated structuring after calcination. The assignment of the hexagonal space group, *P6mm*, was made using the first five Bragg reflections which were fitted using a Gaussian peak shape at q = 0.1702, 0.2948, 0.3404, 0.4503, and 0.5896 $Å^{-1}$ (Figure 2a). The lattice parameter for the twelve replicates ranged from 4.02−4.17 nm with an average value of 4.13 nm (Table 2). This is consistent with the size of the hexagonal liquid crystalline structure of the template surfactant, CTAB, around which the inorganic sol was condensed, 3.2−4.2 nm.[20]

This lattice parameter is also in good agreement with previous literature reports for templated silicate materials synthesized using CTAB as the templating agent, ranging between 3.3 and 4.2 nm.[20,27] The coefficient of variation (CV = σ/μ, where σ is the standard deviation and μ is the mean) for the lattice parameter across the 12 ordered replicates was 1.13%.

The particle size of the samples was also analyzed using DLS to investigate the effect of the miniaturization of sol−gel reactions on the particle size and polydispersity. To accurately determine the size distribution of the particles from the DLS measurements, data treatment was undertaken. This included the removal of outliers using the Grubb's test method from the multiple DLS sizing measurements made for each of the samples. With the outliers removed, the primary particle size

dx.doi.org/10.1021/co300035q | *ACS Comb. Sci.* 2012, 14, 443−450

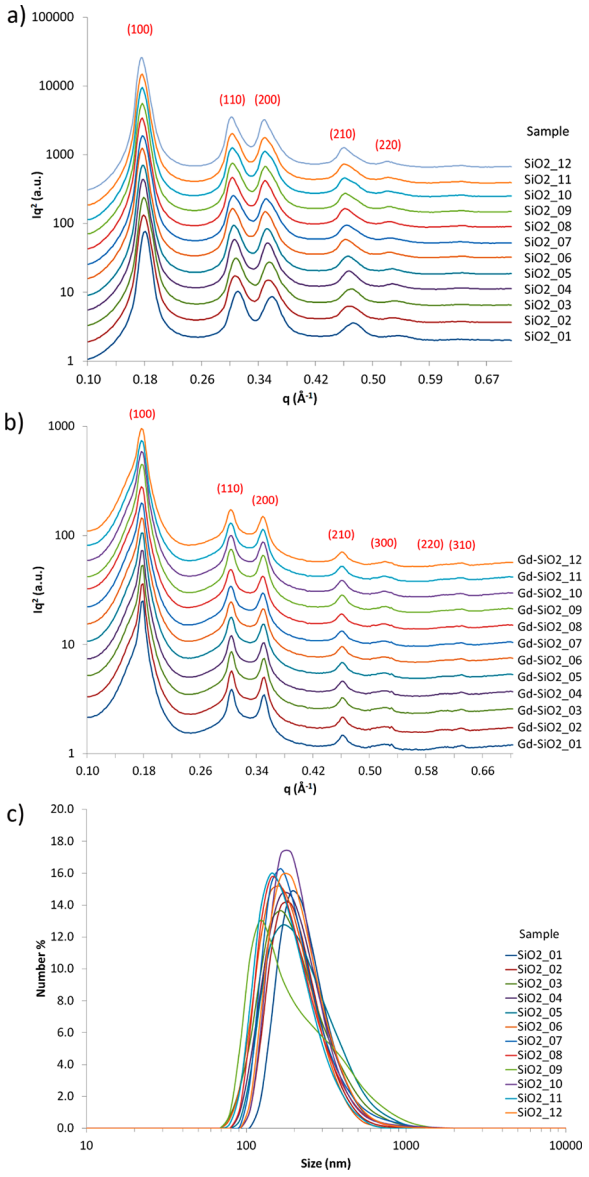

Figure 2. (a) SAXS diffraction patterns for the various silica samples, the Bragg peaks (100), (110), (200), (210), and (300) are labeled at q = 0.1782, 0.3086, 0.3563, 0.4714, and 0.5345 Å^{-1}. The intensity adjusted to the baseline approximated to the polynomial equation of $I = q^{-2}$. (b) SAXS diffraction patterns of the twelve gadolinium doped silicate replicates, with intensity adjusted to the baseline approximated to the polynomial equation of $I = q^{-2}$. The peaks for the Bragg planes (100), (110), (200), (210), (300), (220), and (310) are labeled at q = 0.1742, 0.3016, 0.3484, 0.4608, 0.5225, 0.6034, and 0.6280 Å^{-1}. (c) Stacked plot of the DLS measurements of the twelve mesoporous silica replicates.

was determined and the polydispersity index (PdI) was calculated by taking the standard deviation of the measured values divided by the mean of the peaks. The samples were observed to have a single population with a broad distribution of particle sizes ranging from 80 to 800 nm in particle size (Figure 2c). The range of mean particle sizes for the twelve samples was between 124 and 190 nm with an average across the twelve samples of 165 nm. This variation in the measured particle size is attributed to the experimental variables such as the homogeneity of the solubilization of the CTAB in solution, the calcination temperature due to location within the furnace

Table 2. Summary of the Space Type and Lattice Parameter for the Samples, Determined by SAXS, and the Particle Size and Polydispersity Index (PdI) Determined by DLS

sample	lattice type	lattice parameter[a] (nm)	average particle size (nm)	PdI
SiO_2_01	*P6mm*	4.02	190.1	0.5
SiO_2_02	*P6mm*	4.09	190.1	0.4
SiO_2_03	*P6mm*	4.08	164.2	0.4
SiO_2_04	*P6mm*	4.08	164.2	0.5
SiO_2_05	*P6mm*	4.16	164.2	0.4
SiO_2_06	*P6mm*	4.17	164.2	0.3
SiO_2_07	*P6mm*	4.13	164.2	0.5
SiO_2_08	*P6mm*	4.15	141.8	0.3
SiO_2_09	*P6mm*	4.14	122.4	0.4
SiO_2_10	*P6mm*	4.18	190.1	0.3
SiO_2_11	*P6mm*	4.14	141.8	0.2
SiO_2_12	*P6mm*	4.15	190.1	0.3
mean		4.13	165.6	0.4
standard deviation		0.05	22.2	0.1
coefficient of variation (%)		1.13	13.4	22.6

[a]The lattice parameter for the *P6mm* symmetry was calculated using the formula $a_0 = (2\pi((h^2 + hk + k^2)^{1/2}))/(q_{hk}\sqrt{3})$ where (h,k) are the miller indices of the reflection plane and q_{hk} is the scattering angle for the (h,k) reflection plane.

and subsequent variation in mechanical processes such as grinding and dispersal using sonication. The average PdI for the twelve samples was calculated to be 0.4, indicating that the samples were relatively monodisperse and may be suited for biomedical applications.[28] The CV calculated between the twelve samples was 13.4% and 22.6% for the variation in particle size and PdI, respectively. With only these small variations between the calculated particle sizes and the low PdI of the twelve ordered mesoporous samples, this suggests that the hexagonally ordered sample synthesis with the automated platform was repeatable and reproducible between batches and across different locations of the magnetically stirred temperature controlled MTP.

The process control during the HT synthetic procedure is proposed to be responsible for the small sample-to-sample variation in particle size observed. Sol–gel reactions conducted using the acid–base synthetic route tend to have more monodisperse particles than nanoparticles synthesized using the modified Stöber process. Furthermore, the observed CV is believed to be partly due to slight variation in the heating temperature during the calcination process. The surface of the silica particles are dehydrated during the calcination process as particles which have a high surface curvature are more prone to dehydration. Once this dehydration occurs, the closely associated nanoparticles form weak interparticle Si–O bonds resulting in the formation of necking between the primary particles forming larger aggregates.[28] For this reason there are other known practices to remove the template surfactants, which may avoid sintering and dehydration, including; solvent extraction, hydrogen peroxide treatment and dialysis. The alternative template removal techniques were not studied here as optimization of particle dispersibility was beyond the scope of this work.

SAXS analysis was performed on the gadolinium doped silica replicates. The templated pores retained the hexagonal ordering typically found in MCM-41 materials. From the 7 Bragg reflections observed for the range of materials (Figure 2b) the

dx.doi.org/10.1021/co300035q | *ACS Comb. Sci.* 2012, 14, 443–450

Table 3. Summary of the Lattice Type, Lattice Parameter, Gadolinium Content and the Relaxivity Results for the Twelve Gadolinosilicate Materials

sample	lattice type	lattice parameter[a] (nm)	Gd[b] (wt %)	r_1 (mM^{-1} s^{-1})	r_2 (mM^{-1} s^{-1})
Omniscan	n/a	n/a	n/a	3.01	3.75
Magnevist	n/a	n/a	n/a	4.71	5.30
Gd-SiO_2_01	*P6mm*	4.08	6.39	2.00	7.10
Gd-SiO_2_02	*P6mm*	4.08	5.95	4.14	11.88
Gd-SiO_2_03	*P6mm*	4.08	5.92	2.73	9.36
Gd-SiO_2_04	*P6mm*	4.09	5.61	5.13	15.38
Gd-SiO_2_05	*P6mm*	4.18	5.86	2.78	11.65
Gd-SiO_2_06	*P6mm*	4.19	5.79	2.43	10.12
Gd-SiO_2_07	*P6mm*	4.19	5.88	2.30	11.22
Gd-SiO_2_08	*P6mm*	4.10	5.62	2.92	12.59
Gd-SiO_2_09	*P6mm*	4.02	3.61	3.86	14.63
Gd-SiO_2_10	*P6mm*	4.07	6.69	2.85	13.33
Gd-SiO_2_11	*P6mm*	4.07	7.07	1.81	9.96
Gd-SiO_2_12	*P6mm*	4.07	7.31	2.18	12.75
mean		4.10	5.97	2.93	11.66
standard deviation		0.06	0.93	0.98	2.32
coefficient of variation (%)		1.39	15.62	33.50	19.87

[a]The lattice parameter for the *P6mm* symmetry was calculated using the formula $a_0 = (2\pi((h^2 + hk + k^2)^{1/2}))/(q_{hk}\sqrt{3})$ where (h,k) are the miller indices of the reflection plane and q_{hk} is the scattering angle for the (h,k) reflection plane. [b]Gd content analyzed using LIBS.

Table 4. Summary of Gd-Doped Silica Demonstrating the Influence of Composition on Pore Ordering and MRI Performance

sample	lattice type	lattice parameter [d-spacing] (nm)	Gd^{3+} (wt %)	Al^{3+} (wt %)	r_1 (mM^{-1} s^{-1})	r_2 (mM^{-1} s^{-1})
SiO_2_01	*P6mm*	4.02				
Gd- SiO_2_01	*P6mm*	4.08	6.39		2.00	7.10
Gd-SiO_2_04	*P6mm*	4.09	5.61		5.13	15.38
Gd-Al-SiO_2_01	*P6mm*	3.96	6.41	0.34	2.50	0.60
Gd-Al-SiO_2_02	disordered	[4.16]	5.20	0.55	5.60	0.70
Lin et al.[13]	disordered	[4.32]	6.80		4.4[a]	80.4[a]

[a]Relaxivity measured at 9.4T.

lattice parameters were calculated, Table 3. The lattice parameter ranged from 3.48−3.63 nm with an average of 3.55 nm and CV of 1.4% (Table 3). The addition of gadolinium into the sol−gel reaction improved the ordering of symmetry of the surfactant templated pores, as indicated by the increased number of reflections compared to the nondoped sample and the reduced σ value. The σ values of the Gaussian-fitted (210) reflection peak for both the silicate and gadolinosilicate samples were calculated to be 0.0103 and 0.0060 respectively, using Gaussian full width half-maximum (fwhm) equation (fwhm = $2(2\ \ln\ 2)^{1/2}\sigma$). With this reduced σ, this indicated that the gadolinosilicate samples have a higher long-range ordering in the templated mesoporous structures. The lattice parameter was slightly smaller than the nondoped sample; however this was within the experimental error.

The metal content for the gadolinium-doped samples was analyzed using LIBS. The metal content was relatively consistent between the twelve samples with the exception of Gd-SiO2_09 (Supporting Information Figure S1). This technique is a qualitative measurement technique, which showed that the samples generally have consistent incorporation of metal in the silica matrix.

The MRI performance for the gadolinosilicates was investigated using a 3T commercial MRI scanner.

The average longitudinal and transverse relaxivities for the twelve gadolinosilicate replicates were 2.93 and 11.66 mM^{-1} s^{-1} with a CV of 33.5 and 19.9%, respectively (Table 3). The longitudinal relaxivity was comparable to the commercial CA, Omniscan. Whereas the transverse relaxivity was significantly better. The performance of the gadolinosilicates was also compared with Magnevist (r_1 = 4.71, r_2 = 5.30) and was a more effective T_2 agent then a T_1 agent, similar to Omniscan. This improved performance as a T_2 agent is postulated to be due to the templated pores generated in the gadolinosilicate structure. The added porosity generates a larger specific surface area which may be a more accessible surface for the water to interact and thus via magnetic dipole−dipole interaction, the material has an improved relaxivity performance. The reduced tumbling rate from the nanostructure is also believed to have facilitated the enhanced MR performance. Further work such as relaxometry would elucidate the exact mechanism behind this observed effect including the rotational kinetics of the nanostructure.

In addition to the two reported formulations, two additional silicate samples were synthesized to demonstrate variability in properties with varying compositions. The two gadolinium silicate samples, codoped with aluminum (Gd−Al−SiO_2) were synthesized similarly to the Gd−SiO_2 samples, and both the physical properties and MRI performances were characterized. The structure and properties of these materials were compared to the gadolinosilicates reported herein and similar materials reported previously by Lin et al. (Table 4). The degree of ordering of the templated pores were significantly different depending on the concentration of the Al codopant. The r_1 time was larger for the sample with the higher amount of Al-incorporated. The r_2 time for both the Al doped samples, was

dx.doi.org/10.1021/co300035q | *ACS Comb. Sci.* 2012, 14, 443−450

significantly smaller than those of the Gd−SiO_2 samples. These variations in properties based on low compositional differences reinforce the important role of this HT synthesis and characterization method for the optimization of multivariate sol−gel systems for application as MRI contrast agents.

The HT technique developed has allowed us to readily explore a wide compositional space and to compare structure and property performance relationships. Further work will be undertaken to investigate the optimization of mixed metal doped sol−gel derived materials. Our research group is currently utilizing this technique for the exploration of a variety of sol−gel materials for use as theranostic platforms and other applications which utilize high surface area metal oxides.

To summarize, a method has been developed for the production of mesoporous silica-based nanoparticles including doped mesoporous silicates using a HT robotic synthesis platform, the Chemspeed Accelerator SLTII. The reproducibility of this HT technique was studied with the synthesis of twelve replicates; the structural properties were characterized and compared. Using CTAB as a soft surfactant template, mesoporous silica nanoparticles were generated using an acid−base sol−gel synthesis method. The twelve silica replicates and twelve gadolinosilicates were highly ordered with a *P6mm* hexagonal symmetry. The average lattice parameter was calculated to be 4.13 and 4.10 nm with a coefficient of variation of 1.13 and 1.39% for the silica and gadolinosilicate samples, respectively. At a CTAB/TEOS molar ratio of 0.25, the associated hexagonal pore ordering is consistent with the ordered templating region reported in literature. The gadolinosilicate materials were found to have a mean r_1 and r_2 value of 2.93 and 11.66 mM^{-1} s^{-1}, respectively. The material was comparable to commercial standards, Omniscan and Magnevist as a T_1 contrast agent. Using a suite of HT techniques, we have identified that miniaturization of sol−gel reactions can be achieved and that these techniques can be used for the discovery of novel advanced sol−gel derived nanoparticulate materials for medical imaging CAs.

EXPERIMENTAL PROCEDURES

All chemicals were used without purification and were from Sigma Aldrich unless specified. The preparation of the sol−gel material was undertaken using a Chemspeed Accelerator SLTII robotic synthesis platform by using the layout depicted in Figure 1.

General Procedure for the Preparation of Mesoporous Silica and Gadolinosilicate Nanoparticles. A CTAB chloroform stock solution was prepared (79.16 mg/mL). Prior to loading the vials into the robotic platform, the CTAB stock solution was dispensed using an autopipetter into each of the 2 mL HPLC vials and the solvent was removed in vacuo. The vials were arranged as schematically depicted in Figure 1 and loaded into the aluminum block of the custom MTP heater stirrer located on the Chemspeed Accelerator SLTII. Each vial was loaded with a magnetic stirring bar (10 mm × 3 mm). The reagents ethanol, 1.67 M HCl, and Milli-Q water were added in this order to all vials. The solutions were then mixed and kept at 25 °C and the required amount of tetraethylorthosilicate (TEOS) was added to the vials, one at a time. The mixtures once reacted for 25 min were then quenched. Each mixture was transferred to a quenching vial (50 mL conical base centrifuge tube) on the MTP stage. While vortexing the MTP stage at 530 rpm 6.4 mL of 0.17 M NH_4OH was added at a rate of 20 mL/min. After the addition of the NH_4OH to all of the vials, the MTP stage was vortexed for a further 2 h. The centrifuge tubes containing the precipitated silica sol−gel material were then removed from the robotic system and the nanoparticles were isolated via centrifugation (Genevac vacuum centrifuge) for 3 h at 1000 rpm, washed three times with Milli-Q water and dried in a vacuum desiccator, under active vacuum for 48 h. The isolated nanoparticles were calcined at 500 °C for 10 h under air. The molar reactant composition for preparing the samples was 1(TEOS)/0.250(CTAB)/10.4(ethanol)/22.9(H_2O)/0.67(HCl)/0.98(NH_4OH).

An aqueous stock solution of $GdCl_3 \cdot 6H_2O$ (240 mM) was prepared using Milli-Q water. The gadolinosilicate nanoparticles were prepared using an identical procedure to the silica nanoparticles except for the addition of the gadolinium salt with the reagents: The reagents ethanol, 1.67 M HCl, $GdCl_3$ stock solution, and Milli-Q water were added in this order to all vials. The molar composition for preparing these samples was 1(TEOS)/0.250(CTAB)/0.003(Gd^{3+})/10.4(EtOH)/22.9(H_2O)/0.67(HCl)/0.98(NH_4OH).

The long-range ordering of the synthesized samples was determined using the SAXS beamline at the Australian Synchrotron.[29] The powdered samples were loaded into a custom built multiwell sample holder comprised of a steel plate with dimension of 89 mm × 49 mm × 1 mm with 114, 4 mm diameter wells spaced 1 mm apart and sealed with Kapton tape. The steel plate was loaded into a plate fitting, mounted on the optical stage of the beamline which provided translational motion between samples. Each sample was exposed to the 12 keV X-ray beam, with a dimension of 250 μm × 120 μm and a typical flux of 5 × 10^{12} photons/s, for 1 s. The diffraction patterns were recorded using a Pilatus 1 M detector (Dectris, Switzerland) that was calibrated using silver behenate (*d*-spacing 58.3798 Å). The X-ray wavelength used was 1.0332 Å. The SAXS q range obtained in this configuration was 0.0112 $Å^{-1}$ to 0.7015 $Å^{-1}$. The contribution from an empty well with the kapton tape was subtracted from the scattering profiles and the intensity was normalized to beam stop counts.

DLS was performed using the Malvern Nanosizer (Zetasizer Nano ZS). Milli-Q water was first filtered using a 0.45 μm syringe filter (PALL, Acrodisc Syringe Filters with GHP Membrane). The samples were prepared at ca. 4 mg/mL in water. The samples were agitated and then briefly sonicated to disperse the particles using a bath sonicator (Brandson 5510). The samples were measured at 25 °C assuming a refractive index of 1.475 for the silica particles and the data was analyzed using the DTS software (ver. 5.03). The primary particle population was determined based on the largest peak using the inbuilt algorithm that calculates the number of particles of a given size. This algorithm was chosen and is preferred for these samples due to the presence of a few large aggregates. Multiple measurements were made (n = 6) using an acquisition time of 5 s.

The metal content in the gadolinium doped systems was measured using laser induced breakdown spectroscopy (LIBS, Spectrolaser 4000 from XRF Scientific, Melbourne). The analyses were prepared by adhering ca. 5 mg of sample onto a double sided adhesive tape. The sample was placed onto the LIBS sample holder and the sample was exposed to an Nd:YAG produced laser at 532 nm with a power of 80 mJ per pulse and a spectrometer delay of 0.8 μs. The area under the curve for the gadolinium and silica peak was taken at 341.9−342.6 and 287.8−288.6 nm, respectively. Each sample point was averaged over 30 laser pulses.

dx.doi.org/10.1021/co300035q | *ACS Comb. Sci.* 2012, 14, 443−450

MRI phantom images were obtained of the gadolinosilcate replicates using a Siemens (Germany) 3 T TRIO MRI scanner using a body transmit radio frequency coil and a 12 channel radio frequency receiver coil at the Royal Melbourne Hospital, Victoria, Australia. The samples were prepared first by dispersing ca. 20 mg of sample into 0.5 mL of Milli-Q water followed by sonication. The suspension was then transferred into a polypropylene V-bottom 96-well microtiter plate with 2 mL wells (Porvair Science Ltd., United Kingdom). To each well 0.5 mL of predissolved 0.8 wt % agarose solution was then added. The dispersed sample solution and the agarose solution were triturated using an autopipette to ensure a homogeneous mix, and then gelled in the plate while resting on an ice bath. From the phantom image, the r_1 and r_2 relaxivity values were extracted according to the method reported in the literature.[14]

■ ASSOCIATED CONTENT

Supporting Information

Graphical comparison of the Gd content using LIBS. This material is available free of charge via the Internet at http://pubs.acs.org.

■ AUTHOR INFORMATION

Corresponding Author

*E-mail: danielle.kennedy@csiro.au. Phone: 613 9545 2611.

Notes

The authors declare no competing financial interest.

N.M.K.T. is the recipient of a Commonwealth Scientific and Industrial Research Organisation (CSIRO) PhD studentship. D.F.K. acknowledges the award of a CSIRO Office of the Chief Executive Postdoctoral Fellowship. R.A.C. acknowledges the Australian Research Council for a Future Fellowship (FT0990583). C.J.D. was the recipient of an Australian Research Council Federation Fellowship at the time when this work was conducted.

■ ACKNOWLEDGMENTS

The authors thank Steven Tassios (CSIRO Process Science and Engineering) for performing the LIBS analyses. The authors also acknowledge the Australian Synchrotron where SAXS experiments were undertaken with the assistance of beamline scientists.

■ ABBREVIATIONS

CA, contrast agent; CTAB, cetyltetramethylammonium bromide; CV, coefficient of variation; DLS, dynamic light scattering; HT, high-throughput; LIBS, laser-induced breakdown spectroscopy; MRI, magnetic resonance imaging; MTP, microtiter plate; SAXS, small-angle X-ray scattering; TEOS, tetraethylorthosilicate

■ REFERENCES

(1) Potyrailo, R. A.; Rajan, K.; Stowe, K.; Takeuchi, I.; Chisholm, B.; Lam, H. Combinatorial and High-Throughput Screening of Materials Libraries: Review of State of the Art. *ACS Comb. Sci.* **2011**, *13* (6), 579−633.

(2) Lin, B. B. High throughput screening for new drug discovery. *J. Food Drug Anal.* **1995**, *3* (4), 233−241.

(3) Ebrahimi, D.; Kennedy, D. F.; Messerle, B. A.; Hibbert, D. B. High throughput screening arrays of rhodium and iridium complexes as catalysts for intramolecular hydroamination using parallel factor analysis. *Analyst* **2008**, *133* (6), 817−822.

(4) Kennedy, D. F.; Messerle, B. A.; Rumble, S. L. Application of UV−vis spectroscopy to high throughput screening of hydroamination catalysts. *New J. Chem.* **2009**, *33* (4), 818−824.

(5) Mulet, X.; Kennedy, D. F.; Conn, C. E.; Hawley, A.; Drummond, C. J. High throughput preparation and characterisation of amphiphilic nanostructured nanoparticulate drug delivery vehicles. *Int. J. Pharm.* **2010**, *395* (1−2), 290−297.

(6) Lau, D.; G Hay, D.; R Hill, M.; W Muir, B.; A Furman, S.; F Kennedy, D. PLUXter: Rapid discovery of metal−organic framework structures using PCA and HCA of high throughput synchrotron powder diffraction data. *Comb. Chem. High Throughput Screening* **2011**, *14* (1), 28−35.

(7) Menzies, D. J.; Cowie, B.; Fong, C.; Forsythe, J. S.; Gengenbach, T. R.; McLean, K. M.; Puskar, L.; Textor, M.; Thomsen, L.; Tobin, M. One-step method for generating PEG-Like plasma polymer gradients: Chemical characterization and analysis of protein interactions. *Langmuir* **2010**, No. 17, 13987−13994.

(8) Cawse, J. N. Experimental strategies for combinatorial and high-throughput materials development. *Acc. Chem. Res.* **2001**, *34* (3), 213−221.

(9) Kreiter, R.; Rietkerk, M.; Castricum, H.; van Veen, H.; ten Elshof, J.; Vente, J. Evaluation of hybrid silica sols for stable microporous membranes using high-throughput screening. *J. Sol−Gel Sci. Technol.* **2011**, *57* (3), 245−252.

(10) Na, H. B.; Hyeon, T. Nanostructured T1MRI contrast agents. *J. Mater. Chem.* **2009**, *19* (35), 6233−6428.

(11) Liu, G.; Tse, N. M. K.; Hill, M. R.; Kennedy, D. F.; Drummond, C. J. Disordered mesoporous gadolinosilicate nanoparticles prepared using gadolinium based ionic liquid emulsions: Potential as magnetic resonance imaging contrast agents. *Aust. J. Chem.* **2011**, *64* (5), 617−624.

(12) Jacques, V.; Desreux, J. F., New classes of MRI contrast agents. In *Contrast Agents I*; Springer-Verlag Berlin: Berlin, 2002; Vol. *221*, pp 123−164.

(13) Lin, Y. S.; Hung, Y.; Su, J. K.; Lee, R.; Chang, C.; Lin, M. L.; Mou, C. Y. Gadolinium(III)-incorporated nanosized mesoporous silica as potential magnetic resonance imaging contrast agents. *J. Phys. Chem. B* **2004**, *108* (40), 15608−15611.

(14) Muir, B. W.; Acharya, D. P.; Kennedy, D. F.; Mulet, X.; Evans, R. A.; Pereira, S. M.; Wark, K. L.; Boyd, B. J.; Nguyen, T.-H.; Hinton, T. M.; Waddington, L. J.; Kirby, N.; Wright, D. K.; Wang, H. X.; Egan, G. F.; Moffat, B. A. Metal-free and MRI visible theranostic lyotropic liquid crystal nitroxide-based nanoparticles. *Biomaterials* **2012**, *33* (9), 2723−2733.

(15) Beck, J. S.; Vartuli, J. C.; Roth, W. J.; Leonowicz, M. E.; Kresge, C. T.; Schmitt, K. D.; Chu, C. T. W.; Olson, D. H.; Sheppard, E. W.; McCullen, S. B.; Higgins, J. B.; Schlenker, J. L. A new family of mesoporous molecular-sieves prepared with liquid-crystal templates. *J. Am. Chem. Soc.* **1992**, *114* (27), 10834−10843.

(16) Selvam, P.; Bhatia, S. K.; Sonwane, C. G. Recent advances in processing and characterization of periodic mesoporous MCM-41 silicate molecular sieves. *Ind. Eng. Chem. Res.* **2001**, *40* (15), 3237−3261.

(17) Meynen, V.; Cool, P.; Vansant, E. F. Verified syntheses of mesoporous materials. *Microporous Mesoporous Mater.* **2009**, *125* (3), 170−223.

(18) Yin, W.; Zhang, M. Characterization of nanosized Tb-MCM-41 synthesized by the sol−gel-assisted self-assembly method. *J. Alloys Compd.* **2003**, *360* (1−2), 231−235.

(19) Lin, H. P.; Chi, Y. S.; Lin, J. N.; Mou, C. Y.; Wan, B. Z. Direct synthesis of MCM-41 mesoporous aluminosilicates containing Au nanoparticles in aqueous solution. *Chem. Lett.* **2001**, *11*, 1116−1117.

(20) Naik, B.; Ghosh, N. N. A review on chemical methodologies for preparation of mesoporous silica and alumina based materials. *Recent Pat. Nanotechnol.* **2009**, *3* (3), 213−224.

(21) Kapoor, M. P.; Fujii, W.; Yanagi, M.; Kasama, Y.; Kimura, T.; Nanbu, H.; Juneja, L. R. Environmental friendly rapid mass production synthetic process of highly ordered nanometer sized mesoporous silica

using a combination of acid-base and evaporation approach. *Microporous Mesoporous Mater.* **2008**, *116* (1−3), 370−377.
(22) Fowler, C. E.; Khushalani, D.; Lebeau, B.; Mann, S. Nanoscale materials with mesostructured interiors. *Adv. Mater.* **2001**, *13* (9), 649−652.
(23) Jiang, H.; Gai, L.; Tian, Y. Altervalent cation-doped MCM-41 supported palladium catalysts and their catalytic properties. *J. Serb. Chem. Soc.* **2011**, *00*, 73−73.
(24) de Dood, M. J. A.; Berkhout, B.; van Kats, C. M.; Polman, A.; van Blaaderen, A. Acid-based synthesis of monodisperse rare-earth-doped colloidal SiO_2 spheres. *Chem. Mater.* **2002**, *14* (7), 2849−2853.
(25) Pope, E. J. A.; Mackenzie, J. D. Sol-gel processing of silica. II: The role of the catalyst. *J. Non-Cryst. Solids* **1986**, *87* (1−2), 185−198.
(26) Brinker, C. J.; Scherer, G. W., *Sol−Gel Science: The Physics and Chemistry of Sol−Gel Processing*, 1st ed.; Academic Press: 1990; p 912.
(27) Nooney, R. I.; Thirunavukkarasu, D.; Chen, Y.; Josephs, R.; Ostafin, A. E. Synthesis of nanoscale mesoporous silica spheres with controlled particle size. *Chem. Mater.* **2002**, *14* (11), 4721−4728.
(28) Rahman, I. A.; Vejayakumaran, P.; Sipaut, C. S.; Ismail, J.; Chee, C. K. Effect of the drying techniques on the morphology of silica nanoparticles synthesized via sol−gel process. *Ceram. Int.* **2008**, *34* (8), 2059−2066.
(29) Kirby, N.; Boldeman, J.; Gentle, I.; Cookson, D. *Conceptual Design of the Small Angle Scattering Beamline at the Australian Synchrotron* **2007**, 887.